

Exploring the Multi-Mode Structure of Atom-Generated Squeezed Light

A thesis submitted in partial fulfillment of the requirement
for the degree of Bachelor of Science in Physics from
The College of William and Mary


by

Melissa Anne Guidry

Accepted for Honors
(Honors or no-Honors)


Eugeny Mikhailov, Director

Gina L. Hoatson
Gina Hoatson, Physics


Junping Shi, Mathematics

Williamsburg, VA
April 28, 2017

Exploring the Multi-Mode Structure of Atom-Generated Squeezed Light

by

Melissa Anne Guidry

Submitted to the Department of Physics
on April 28, 2017, in partial fulfillment of the
requirements for the degree of
Bachelor of Science in Physics

Abstract

Squeezed states of light, *i.e.*, quantum states exhibiting reduced noise statistics, may be used to greatly enhance the sensitivity of light-based measurements. We study a squeezed vacuum field generated in hot Rb vapor via the polarization self-rotation effect. By propagating a strong pump beam through an atomic vapor cell, we were able to achieve a noise suppression of 2.7 dB below shot noise. Our previous work revealed that this amount of noise suppression may be limited by the excitement of higher order modes in the squeezed field during the atom-light interaction. Once incident on the homodyne detection scheme, these higher order modes may induce an imperfect mode match between the squeezed field and the local oscillator (LO). In this work, we used a liquid-crystal-based spatial light modulator to modify the spatial mode structure of the pump and LO beams. We demonstrate that optimization of the spatial modes can lead to higher detected noise suppression.

Thesis Supervisor: Eugeny E. Mikhailov

Title: Assistant Professor

Acknowledgments

Foremost, I would like to express my sincerest gratitude to my advisor, Professor Eugeny Mikhailov, who kept a sense of humor when I had lost mine. His support and guidance were truly extraordinary. I would like to thank Professor Irina Novikova for offering invaluable advice at the inevitable roadblocks. I would also like to thank Dr. Mi Zhang and Demetrious Kutzke for their patience and guidance in the lab. Additionally, I thank all of my group members for their endless support. This research was supported by the Virginia Space Grant Consortium and the Air Force Office of Scientific Research.

Contents

1	Introduction	5
1.1	Quantum noise and squeezed light	5
1.2	Applications of squeezed light	6
1.3	Squeezing with resonant atoms	7
2	Theory	9
2.1	Quantum fluctuations	9
3	Detection scheme	12
3.1	Homodyne detection	12
3.2	Experimental setup	13
3.3	Signal analysis	15
4	Multi-mode generation	17
5	Spatial mode optimization	21
5.1	Pump beam optimization	21
5.2	Local oscillator optimization	25
6	Quantum imaging	27
6.1	Twin beam subtraction	28
6.2	Kinetic mode subtraction	31
7	Conclusions and outlook	32

Chapter 1

Introduction

Squeezed light is a nonclassical state of the electromagnetic field, where the photon statistics differ from those of coherent light. These states act as a powerful tool to reduce the uncertainty in many optical precision measurements. In addition to a wealth of technical applications, manipulation of the quantum noise in squeezed states adds another dimension to the study of electromagnetic radiation and the quantum mechanical structure of nature.

1.1 Quantum noise and squeezed light

One of the foundations of quantum mechanics is the Heisenberg Uncertainty Principle, which states that certain pairs of observables in a system cannot be known simultaneously to better than a certain precision. Via the quantum description of light, we define an uncertainty relation between the amplitude (ΔX_1) and phase (ΔX_2) quadratures of the electromagnetic field: $\Delta X_1 \Delta X_2 \geq 1/4$. This implies that one cannot know the exact amplitude and phase of light simultaneously. Hence, we observe a fundamental limiting noise on any light-based measurement.

For coherent states of light, the quantum uncertainties in the amplitude and phase quadratures are equal. The quantum noise of each quadrature is known as the **standard quantum limit** or **shot noise**, and can be thought of as arising from the discrete nature of photons. This noise exists even in the vacuum state; vacuum fluc-

tuations are *the* source of fundamental noise on a signal of interest.

To go beyond shot noise limited measurements, we look to nonclassical states of light called **squeezed states**, where we can manipulate the quantum noise. The Heisenberg Uncertainty Principle only places a limit on the combination of uncertainties of the amplitude and phase of light. Hence, if the quantum uncertainty in the amplitude is reduced, the phase uncertainty is increased. This “squeezing” of one uncertainty and “stretching” of the other may be achieved in quantum squeezed states. By building correlations between the amplitude and phase of the light using higher order nonlinear interactions with atoms, these squeezed states may be readily generated.

1.2 Applications of squeezed light

One natural application of squeezing is in precision optical measurements. Any shot-noise-limited optical measurement can potentially be improved by the reduced uncertainty levels of a squeezed state. For many measurements, the increased uncertainty of one property is no problem if we are only interested in measuring the other property of the light.

One important use for squeezed light is to improve the sensitivity of interferometric measurements, as suggested by Caves [1]. More topically, squeezing can be used to improve the most sensitive interferometric detector in the world in the LIGO experiment for detection of gravitational waves. One of the dominant sources of noise in the quantum-limited LIGO interferometer is caused by the vacuum fluctuations that enter into the empty port of a beamsplitter. This vacuum noise becomes the limiting source of noise across an important range of gravitational wave frequencies. If this vacuum state is replaced by a squeezed vacuum state, the fluctuations of the measured quadrature can be reduced, resulting in an overall more precise measurement. Squeezed vacuum has already been utilized in GEO600: Using vacuum squeezed 2 dB below shot noise, the sensitivity of the detector was improved by 26% [2]. Hence, one of the main improvements for the next generation LIGO comes from using squeezed

vacuum.

Other interferometric measurements, such as those used for measuring polarization, can show improvements in precision [3]. Absorption measurements that depend on amplitude modulation may be improved by decreasing amplitude noise which boosts the signal-to-noise ratio [4]. Additionally, squeezed light can be used to improve a wide range of atomic spectroscopy measurements [5]. Other examples could include improvements in optical magnetometers, frequency standards, timekeeping, and biological measurements. These applications and more may take advantage of the manipulation of signal noise using squeezed states of light.

1.3 Squeezing with resonant atoms

In this report, we focus on squeezed vacuum produced in atomic vapors through a nonlinear light-atom interaction known as polarization self-rotation (PSR). Atoms provide a broad range of possibilities due to our ability to manipulate and tune light interactions with atomic vapors. Techniques shown to produce squeezing in atoms include four-wave mixing, the nonlinear Kerr effect, and PSR.

The PSR technique offers several advantages over other squeezing generation schemes. The method is simple: Squeezed vacuum can be generated via PSR using only a diode laser and an atomic vapor cell in a single-pass configuration. The power requirements are low, on the order of milliwatts, and the setup has the potential to be easily miniaturized. Squeezing is produced without the use of an atomic cavity and the vacuum may be separated from the pump using polarizers or beam splitters. The strength of the interaction may be tuned to fit the experiment by changing light intensity and atomic density, and the temperature ranges necessary are easily achieved. Overall, PSR squeezing offers a source of squeezed vacuum which is much less complicated, less costly, and potentially more stable than most other squeezing methods.

In the PSR effect, the polarization of a near-resonant beam of light rotates as it travels through a material that is circularly birefringent. Given a strong pump beam

that is linearly polarized, small rotations in this beam can project changes onto the vacuum state in the orthogonal polarization, which are correlated in such a way as to produce squeezed vacuum.

In 2002, polarization self-rotation squeezing in atomic vapors was studied in the theoretical work by Matsko *et al.* [6]. The authors predicted that squeezing levels as high as -8 dB below shot noise could be achieved using this method in hot Rb atoms. The best atomic PSR squeezing reported has been a noise suppression of -3 dB. These observations below theoretical predictions are possibly due to the mode composition of the squeezed field. During the light-atom interaction, higher order modes are generated in the squeezed vacuum. This may lead to a mode mismatch between the squeezed vacuum and the local oscillator, reducing observed squeezing [7]. In this report, we present the results of experimental studies into the mode structure of the pump and local oscillator used for squeezing.

Chapter 2

Theory

2.1 Quantum fluctuations

When we quantize the electromagnetic field, we represent the electromagnetic field operator in terms of the creation and annihilation operators [8]. For simplicity, we focus on a linearly polarized plane wave

$$\hat{E} = E_0(z) \left(\hat{a} e^{-i\omega t} + \hat{a}^\dagger e^{i\omega t} \right)$$

where E_0 is the spatially-dependent amplitude and ω is the frequency of the field. Alternatively, we may represent the field in terms of quadrature operators \hat{X}_1 and \hat{X}_2 ,

$$\hat{X}_1 = \frac{1}{2}(\hat{a} + \hat{a}^\dagger) \tag{2.1}$$

$$\hat{X}_2 = \frac{1}{2i}(\hat{a} - \hat{a}^\dagger) \tag{2.2}$$

In this form, it is apparent that these operators return the real and imaginary components of the electromagnetic field, oscillating with frequency ω and a $\pi/2$ phase difference:

$$\hat{E}_x = 2E_0(z) \left(\hat{X}_1 \cos \omega t + \hat{X}_2 \sin \omega t \right)$$

These operators are Hermitian and correspond to observables. Additionally, using Eq. 2.1, 2.2 we find that the quadrature operators are non-commutative

$$[\hat{X}_1, \hat{X}_2] = \frac{i}{2}$$

allowing us to define an uncertainty limit on quadrature variance via the Schrodinger uncertainty relation:

$$\langle(\Delta\hat{X}_1)^2\rangle\langle(\Delta\hat{X}_2)^2\rangle \geq \frac{1}{16} \quad (2.3)$$

We may calculate the expectation value of the quadrature variance in the coherent states (*i.e.*, ordinary laser light), and we find that it is a minimum uncertainty state such that

$$\langle(\Delta\hat{X}_1)^2\rangle = \langle(\Delta\hat{X}_2)^2\rangle = \frac{1}{4} \quad (2.4)$$

We refer to this state as the standard quantum limit (SQL), where the noise is referred to as shot noise. In Fig. 2-1, the coherent state is represented in the first phase diagram. Here, the “ball” of noise is a perfect circle, representing two equal quadrature noises. The distance from the origin represents the amplitude of the coherent field whereas the angle θ represents the phase. This noise has a tendency to limit light-based measurements where classical noise sources have been nearly eliminated. However, this is not the end of the story. Via squeezed states, we can squeeze one noise quadrature while stretching the other. This is represented as the second image in Fig. 2-1. The ball of noise has been stretched and there exists a measurement along the ball of noise such that, for the squeezed quadrature, $\Delta X_{sq} < 1/2$.

In our work, we specifically study squeezed vacuum. Via our quantization of the electromagnetic field, we define a vacuum state to be a quantum light state with a photon number state of zero photons $|0\rangle$ such that, on average, the light field has zero amplitude $\langle 0 | \hat{E} | 0 \rangle = 0$. Contrary to a classical picture of light, the vacuum state has

nonzero quadrature fluctuations

$$\langle 0 | (\Delta \hat{X}_1)^2 | 0 \rangle = \langle 0 | (\Delta \hat{X}_2)^2 | 0 \rangle = \frac{1}{4}$$

This is equivalent to the coherent state. Hence, we find that a naturally occurring vacuum state $|0\rangle$ is in fact coherent vacuum. The existence of a coherent vacuum with nonzero fluctuations leads to peculiar phenomena. For example, when a beam is coupled into a single input port of a beam splitter, naturally occurring coherent vacuum couples into the second input port, potentially adding noise to the measurement. We may stretch these noise fluctuations like before, herein creating a squeezed vacuum. A representation of coherent vacuum and squeezed vacuum may be seen in Fig. 2.1. For a more in-depth treatment of squeezed states, see Reference [9].

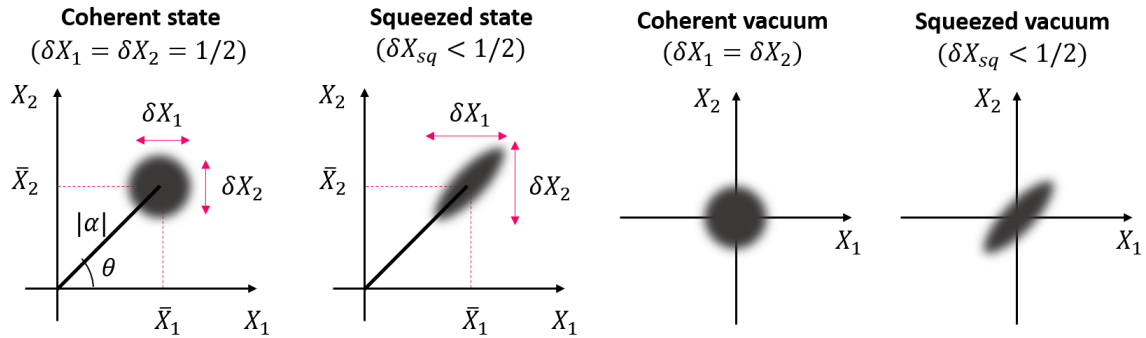


Figure 2-1: Phase diagrams of different quantum states with illustrated quadrature fluctuations.

Chapter 3

Detection scheme

3.1 Homodyne detection

The quadrature operators \hat{X}_1 and \hat{X}_2 correspond to direct observables such that the noise power of the amplitude and phase quadratures (respectively) may be measured. However, this requires a phase-adjustable measurement to probe the quadrature that is being squeezed ($\Delta X_{sq} < 1/2$). Another problem to overcome is the very weak signal of squeezed vacuum; we need to amplify the quadrature noise signal to an intensity above electronic noise.

To overcome these challenges, we utilize a **balanced homodyne detection** scheme. In this scheme, the weak signal of interest is mixed with a strong local oscillator (LO) beam on a 50/50 beamsplitter. The two outputs of the beamsplitter are then sent to two identical photodiodes. The photodiode signals are then subtracted: this is referred to as a balanced photodetector (see Fig. 3-1).

We first consider two classical fields, a weak signal of interest with amplitude $\mathcal{E}_s(t)$ and a strong local oscillator with both an amplitude $\mathcal{E}_{LO}(t)$ and an arbitrary phase $e^{i\theta}$ compared to the signal of interest. We can represent these amplitudes as

$$\mathcal{E}_s(t) = \mathcal{E}_s + \delta X_{1,s}(t) + \delta X_{2,s}(t) \quad (3.1)$$

$$\mathcal{E}_{LO}(t) = [\mathcal{E}_{LO} + \delta X_{1,LO}(t) + \delta X_{2,LO}(t)]e^{i\theta}, \quad (3.2)$$

where \mathcal{E}_s and \mathcal{E}_{LO} are the mean-valued amplitudes, and $X_1(t)$ and $X_2(t)$ represent respective time-varying quadrature fluctuations. When the beams are combined and split on a 50/50 beam splitter, the output signals are the same except for a phase shift introduced by the beam splitter:

$$\mathcal{E}_1 = \sqrt{1/2}\mathcal{E}_{LO}(t) + \sqrt{1/2}\mathcal{E}_s(t) \quad (3.3)$$

$$\mathcal{E}_2 = \sqrt{1/2}\mathcal{E}_{LO}(t) - \sqrt{1/2}\mathcal{E}_s(t). \quad (3.4)$$

The photodiodes measure the intensity of the fields, which are proportional to the squares of the amplitudes $|\mathcal{E}_1|^2$ and $|\mathcal{E}_2|^2$. Taking a first order approximation,

$$|\mathcal{E}_1|^2 - |\mathcal{E}_2|^2 \approx 2\mathcal{E}_{LO}(\delta X_{1,s} \cos \theta + \delta X_{2,s} \sin \theta) \quad (3.5)$$

The variance of this signal is proportional to

$$4\mathcal{E}_{LO}^2[\delta X_{1,s}^2 \cos^2 \theta + \delta X_{2,s}^2 \sin^2 \theta]. \quad (3.6)$$

With homodyne detection, the quadrature fluctuations of the signal of interest are amplified by the amplitude of the local oscillator. This allows us to raise the noise level of our measurement above electronic noise. By controlling the phase θ of the local oscillator compared to the signal, we can select the noise quadrature that we measure. For $\theta = 0$, we measure only $X_{1,s}$. For $\theta = \pi/2$, we measure only $X_{2,s}$.

3.2 Experimental setup

Our experiment is carried out with squeezed vacuum generated in hot atomic ^{87}Rb vapor cells. In this section, we describe the experimental setup of our hot atomic squeezer (see Fig. 3-1). The output of a diode laser was tuned near the $5^2S_{1/2}, F = 2 \rightarrow 5^2P_{1/2}, F' = 2$ transition of ^{87}Rb ($\lambda \approx 795$ nm). We sent the laser beam through a single-mode optical fiber followed by a polarizer to prepare a high quality linearly polarized pump beam with a Gaussian transverse profile. This pump beam was then

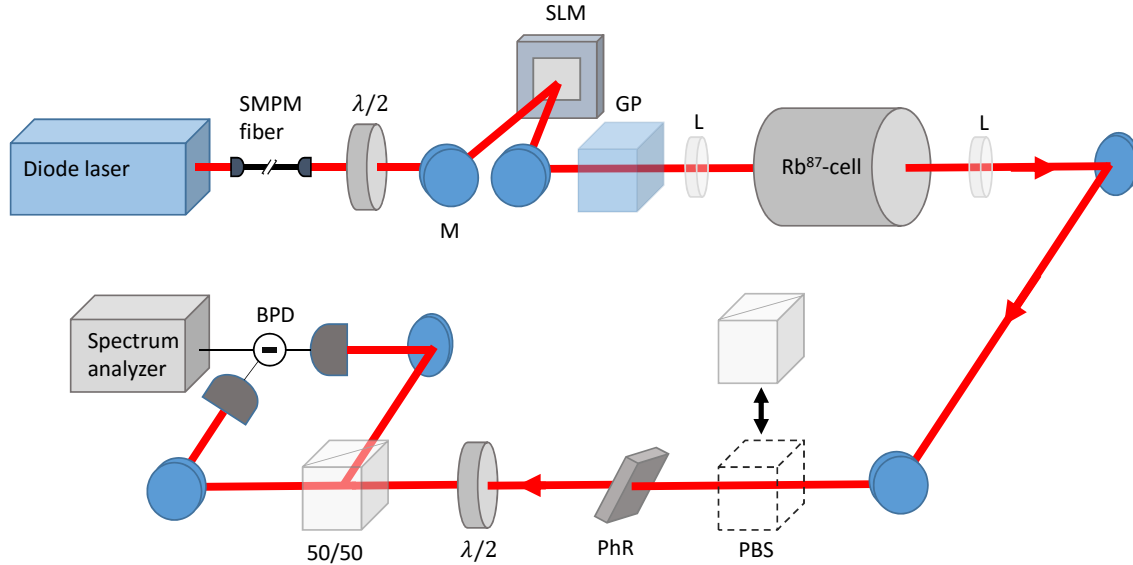


Figure 3-1: The experimental setup for measuring squeezing and shot noise. We employ the following symbols: *SMPM* (Single mode polarization maintaining fiber), $\lambda/2$ (Half-wave plate), *M* (Mirror), *SLM* (Spatial light modulator), *GP* (Glenn polarizer), *L* (Lens), *PBS* (Polarizing beam splitter), 50/50 (50/50 beam splitter), and *BPD* (Balanced photodiode).

focused inside a 7.5 cm long cylindrical Pyrex cell with isotopically enriched ^{87}Rb vapor without buffer gas. The focal lengths of the lenses before and after the cell were adjusted to produce maximal squeezing. The vapor cell was mounted inside a three-layer magnetic shielding and the number density of Rb atoms (always on the order of 10^{11} to 10^{12} cm^{-3}) was varied by adjusting the cell temperature. The input laser power in the cell was controlled by rotating a half wave plate before the polarizer.

We use a detection scheme such that the LO and squeezed vacuum field are never separated, allowing for theoretically perfect overlap of their spatial profiles. After interaction with the atoms, the two fields initially have orthogonal linear polarizations. The polarizations are then rotated by 45° with respect to the axis of a polarizing beam splitter (PBS) using a half-wave plate. Hence the PBS splits the beam with an equal 50/50 ratio, and each separated beam consists of the same amount of local oscillator and squeezed vacuum intensities. After the PBS, the two split laser beams are directed to the balanced photodiode.

To change the relative phase θ of the LO with respect to the vacuum, we send

the beams through a phase-retarder. We use a quarter wave plate before the half-wave plate and align it such that the ordinary and extraordinary axes coincide with the laser beam polarizations. The alignment allows a phase shift for light of one polarization without affecting the orthogonally-polarized light. In this arrangement, a small rotation of the quarter-wave plate introduces a controllable phase shift between the squeezed vacuum and the LO beam.

To calibrate the shot noise, a PBS is inserted into the beam path before the quarter-wave plate and set such that all of the squeezed vacuum is ejected and replaced with coherent vacuum. Weak absorption in the polarizer produces a small loss, decreasing the shot noise level by nearly 0.2 dB. However, this correction is easily taken into account. In the following sections, the measured squeezing is taken to mean the squeezing on the noise quadrature where the measured noise is maximally below shot noise.

A spatial light modulator (SLM) is inserted either before or after the atomic cell to manipulate the spatial profile of the beam (discussed in Chapter 4: Multi-mode generation).

3.3 Signal analysis

To measure noise levels, we analyze the noise spectrum of the signal from the homodyne detection (Eq. 3.6). To measure the noise power at different detection frequencies, the spectral variance of the current from the photodetectors is measured using a spectrum analyzer.

The spectrum analyzer combines the input current with an internally generated oscillating signal to measure the beat frequency power. This allows us to probe the amplitudes of sinusoidal modulations at specific frequencies. The mixed signal passes through a narrowband filter per the resolution bandwidth. The final output is averaged over time before being displayed. The noise power spectrum is most often

displayed as a power ratio on a logarithmic scale in decibels,

$$dB = 10 \log_{10}(P/P_{ref}), \quad (3.7)$$

where P is the power of the signal of interest and P_{ref} is the power of a reference signal. In this way, the noise power in a signal may be displayed as a function of frequency.

When taking a squeezed noise measurement, shot noise is first measured by mixing the local oscillator with coherent vacuum. The squeezed noise level is then measured by comparing the relative noise powers of the signal to the shot noise level. A squeezing level of -10 dB corresponds to noise that is reduced by a factor of 10. Our highest measured squeezing to date has been -2.7 dB, comparable to the world record using these methods [10].

Chapter 4

Multi-mode generation

All previous experimental and theoretical analyses of PSR squeezing have assumed an identical single spatial mode for both the strong pump and vacuum fields, particularly limited to the Laguerre-Gaussian (LG) [10, 11] transverse profiles. The LG mode basis is a natural basis for our system, as it exhibits cylindrical symmetry. The expression of the field distribution for Laguerre-Gaussian modes is

$$\begin{aligned} LG_{p,l} = u_{p,l}(r, \phi, z) &= \frac{C_{lp}^{LG}}{w(z)} \left(\frac{r\sqrt{2}}{w(z)} \right)^{|l|} \exp\left(-\frac{r^2}{w^2(z)}\right) \\ &L_p^{|l|} \left(\frac{2r^2}{w^2(z)} \right) \exp\left(-ik\frac{r^2}{2R(z)}\right) \exp(il\phi) \\ &\exp[i(2p + |l| + 1) \arctan(z/z_R)] \end{aligned} \quad (4.1)$$

where l is the radial index and p is the azimuthal index.

When we theoretically describe the homodyne detection, we assume that the LO and the squeezed vacuum field have the same spatial distribution. However, if the two fields have nonequal spatial dependencies in the amplitude and phase distributions, we describe the two states

$$\begin{aligned} \mathcal{E}_s(t) &= [\mathcal{E}_s + \delta X_{1,s}(t) + i\delta X_{2,s}(t)] u_s(x, y) e^{i\phi(x,y)} \\ \mathcal{E}_{LO}(t) &= [\mathcal{E}_{LO} + \delta X_{1,LO}(t) + i\delta X_{2,LO}(t)] u_{LO}(x, y) e^{i\theta} e^{i\phi'(x,y)} \end{aligned}$$

in terms of the amplitude distributions $u_s(x, y)$ and $u_{LO}(x, y)$, as well as the respective phase distributions $e^{i\phi(x,y)}$ and $e^{i\phi'(x,y)}$. The variance of the signal on the homodyne detection then reads

$$\begin{aligned} \Delta I_-^2 \approx & \mathcal{E}_{LO}^2 \delta X_{1,s}^2 \left[\iint |u_{LO} u_s^* + u_{LO}^* u_s| \cos(\chi) dx dy \right]^2 \\ & + \mathcal{E}_{LO}^2 \delta X_{2,s}^2 \left[\iint |u_{LO} u_s^* + u_{LO}^* u_s| \sin(\chi) dx dy \right]^2 \\ & + \left(1 - \frac{1}{2} \iint |u_{LO} u_s^* + u_{LO}^* u_s|^2 dx dy \right) \mathcal{E}_{LO}^2 \delta X_{1,2v}^2 \end{aligned} \quad (4.2)$$

where $\chi = (\phi + \phi' + \theta)$. We find that the detected signal no longer has a simple dependence on the phase difference θ . Now, we worry about coherent vacuum $\delta X_{1,2v}^2$ coupling into our detector and substantially decreasing the amount of squeezing we observe.

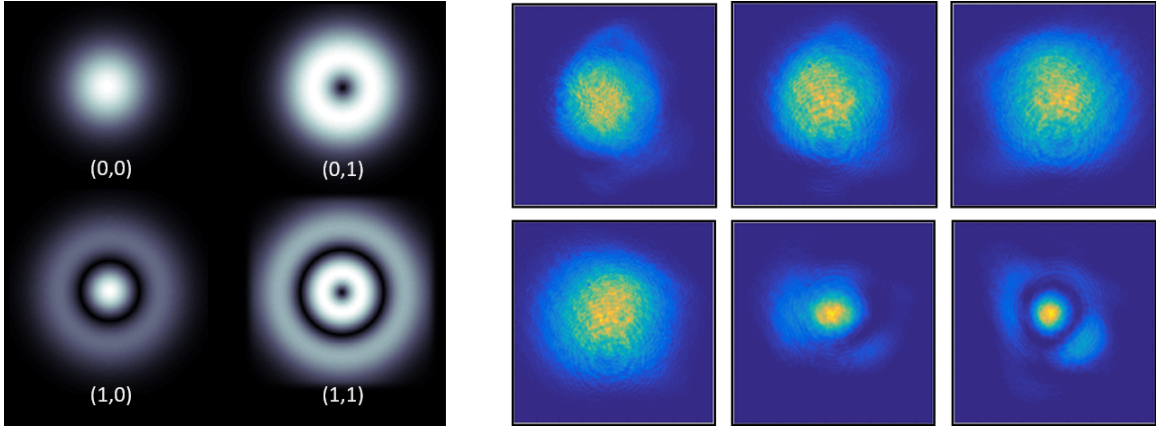


Figure 4-1: Left: The first four Laguerre-Gaussian mode intensity distributions, distinguished by the mode numbers (p, l) . Right: The intensity profiles of the local oscillator after interaction with atoms. The atomic density of the medium increases from $1.4 \times 10^{10} \text{ cm}^{-3}$ to $1.1 \times 10^{13} \text{ cm}^{-3}$ from left to right. The bottom left image corresponds to the atomic density that leads to optimal squeezing. The bottom right image corresponds to the highest atomic density interaction and degraded squeezing.

If the pump, local oscillator, and squeezed fields all remained in the same LG_{00} mode (Fig. 4-1, left), we need not worry about mode mismatch in the homodyne detection. However, we have reason to believe that they do not. Previous experiments in our group revealed the strong dependence of squeezing on spatial structure. Specif-

ically, applying spatial ring masks to the squeezed field degrades squeezing beyond the theoretical predictions for a beam with no spatial dependence [7].

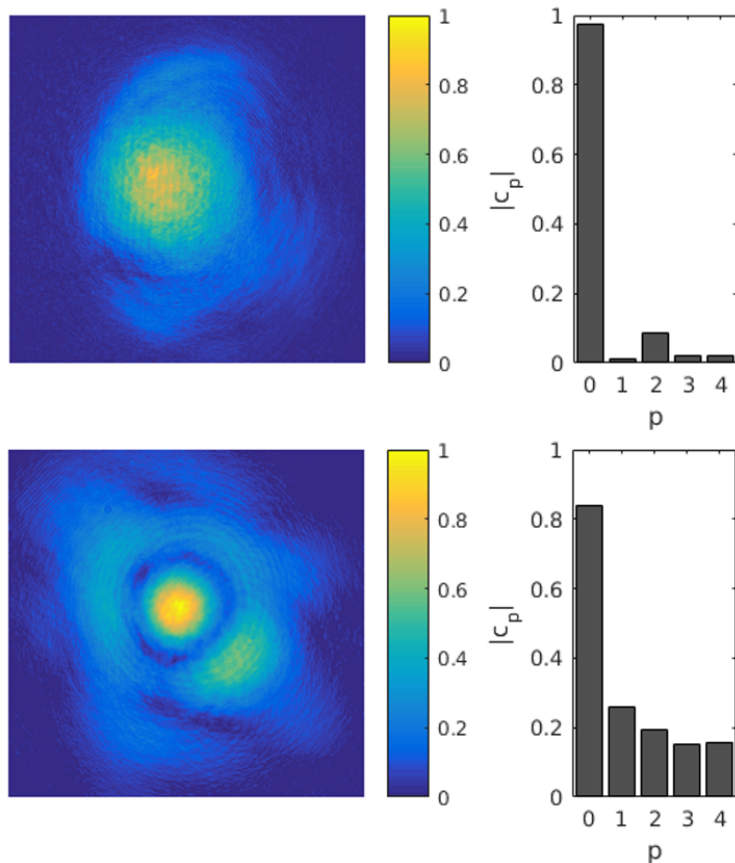


Figure 4-2: LG mode decomposition of a low atomic interaction beam (top) and a high atomic interaction beam (bottom). The LG mode coefficients for each beam are displayed.

A theoretical model that incorporates the possibility of different spatial modes predicts that during the PSR light-atom interaction, the first five LG modes where ($p = 0, 1, 2, 3, 4; l = 0$) will be generated in the squeezed field [7]. Moreover, the different modes may squeeze by different amounts and at different squeezing angles θ . The combination of these different squeezing angles may degrade overall detected squeezing.

Using a quantum noise-limited camera (described in Chapter 6: Quantum imaging), we monitored the intensity distribution of the local oscillator as the atomic density was increased (Fig. 4-1, right). Here, higher atomic density corresponds to a

stronger nonlinear PSR effect. The first frame corresponds to the image of the input Gaussian pump beam after traveling through the atomic cell with low atomic density. We see that it interacts with the atoms very weakly, if it at all. As the atomic density is increased via an increase in temperature, the beam grows wider. At high atomic density, distinct higher order LG modes dominate the intensity distribution and squeezing is degraded.

The LG modes form a complete basis: any image may be decomposed using a linear combination of LG modes. By taking an overlap integral between the image and the first few LG modes, we are able to identify the coefficients of the modes in the mode decomposition (Fig. 4-2). We find that the beam which passes through the minimal atomic density ($1.4 \times 10^{10} \text{ cm}^{-3}$) is primarily composed of the Gaussian mode (LG_{00}). The beam that has passes through the maximal atomic density ($1.1 \times 10^{13} \text{ cm}^{-3}$) is composed of several higher order modes, as expected.

Chapter 5

Spatial mode optimization

5.1 Pump beam optimization

Previous measurements conducted by our group have shown that squeezing may be improved by using an optimal mode structure of the pump beam incident on the atoms [7]. By using the local oscillator from one atomic cell as the pump beam for a second atomic cell, squeezing may be substantially improved. This motivates our search for an optimized pump beam mode structure. While a fundamental Gaussian mode structure is typically used for the pump beam, there may exist a mode structure that induces fewer higher order modes and thus preserves squeezing.

To control the transverse phase profile of the pump beam, we reflect it off of the surface of a liquid-crystal-based spatial light modulator (SLM) before sending it into the atomic cell (see Fig. 3-1). An SLM is an electrically programmable device that modulates light phase according to a spatial pattern. In our case, we are specifically modulating the relative phase of each pixel, with a pixel area of 15×15 microns. By electrically controlling the individual phase shift of each pixel and reflecting our beam off of the surface of the SLM, we can subject our beam to arbitrary phase shift profiles.

After calibrating our SLM using a phase-modulating method, we began looking to alter the phase distribution of the pump beam to optimize the squeezing factor of the squeezed vacuum. We have thus-far studied an optimization method where the

coefficients of Laguerre-Gaussian modes are altered until squeezing is optimized. By projecting the phase distribution of this equation for a specific mode onto the SLM, we may recreate the phase distribution in the beam associated with that mode. In Fig. 5-1, different intensity distributions for LG modes are plotted with the associated phase distributions. Using this technique, we have been able to recreate beams with identical phase distributions.

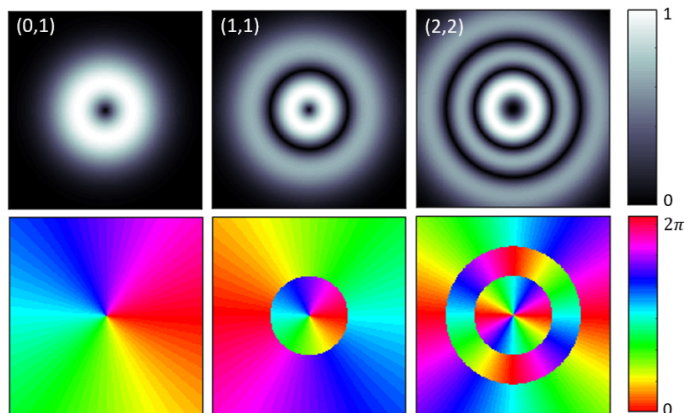


Figure 5-1: Top: The normalized intensity distributions for three different LG modes. Bottom: The phase distributions associated with the mode intensity distributions directly above.

Our LG mode optimization employs a Metropolis-type annealing algorithm. In 1953, Metropolis, Rosenbluth, and Teller devised an algorithm which can mimic the distribution of system states according to energies of the states and the overall temperature of the physical system via the Boltzmann energy distribution law. This law states that the probability to find a state with energy E is given by

$$p(E) \sim \exp\left(-\frac{(E - E_0)}{k_B T}\right), \quad (5.1)$$

where k_B is the Boltzmann constant, E_0 is the minimum energy state, and T is the temperature of the system. When $E = E_0$, the probability of this state is $p(E) = 1$. As E grows larger than E_0 , the probability decreases.

The goal of the algorithm is to reach the minimum “energy” state of the system.

In our experiment, energy is replaced by the detected squeezing factor. Our algorithm functions as follows:

1. Initialize the system to a value such that $k_B T$ is larger than the energy function fluctuation.
2. Assign a beam waist w and a vector of real and imaginary coefficients $[c_1, c'_1, \dots, c_N, c'_N]$ for N LG modes.
3. Set the SLM to correspond to the phase of the LG mode pattern. The phase mask applied to the beam is

$$\Phi(x, y) = \arg \left(\sum_{p,l}^N (c_{pl} + ic'_{pl}) LG_{pl}(w, x, y) \right) \quad (5.2)$$

where LG_{pl} is the mode distribution, w is the beam waist, and c_{pl} , c'_{pl} are coefficients for mode (p, l) . The mode distribution generated via the LG mode equation, Eq. 4-1.

4. Measure the squeezing, E , using this mask.
5. Change the LG mode parameters.
6. Reset the SLM and measure the new squeezing, E_{new} .
7. If $E_{new} < E$, then accept the new parameters and set $E = E_{new}$. If $E_{new} > E$, then we accept the new parameters with the probability

$$p = \exp \left(- \frac{(E_{new} - E)}{k_B T} \right).$$

8. Decrease the temperature.
9. Repeat steps 5-8 for a given number of cycles.

Given enough cycles, an approximate global optimum may be reached. The advantage of this algorithm is its probabilistic acceptance of worse solutions, which allows for a more extensive search for the optimal solution. In this way, the algorithm is less likely to be locked into a local minimum.

Our optimization routine was run with several different combinations of modes in the parameter space. However, only higher order p-mode studies are reported below. We compared the optimized squeezing of two different parameter space compositions:

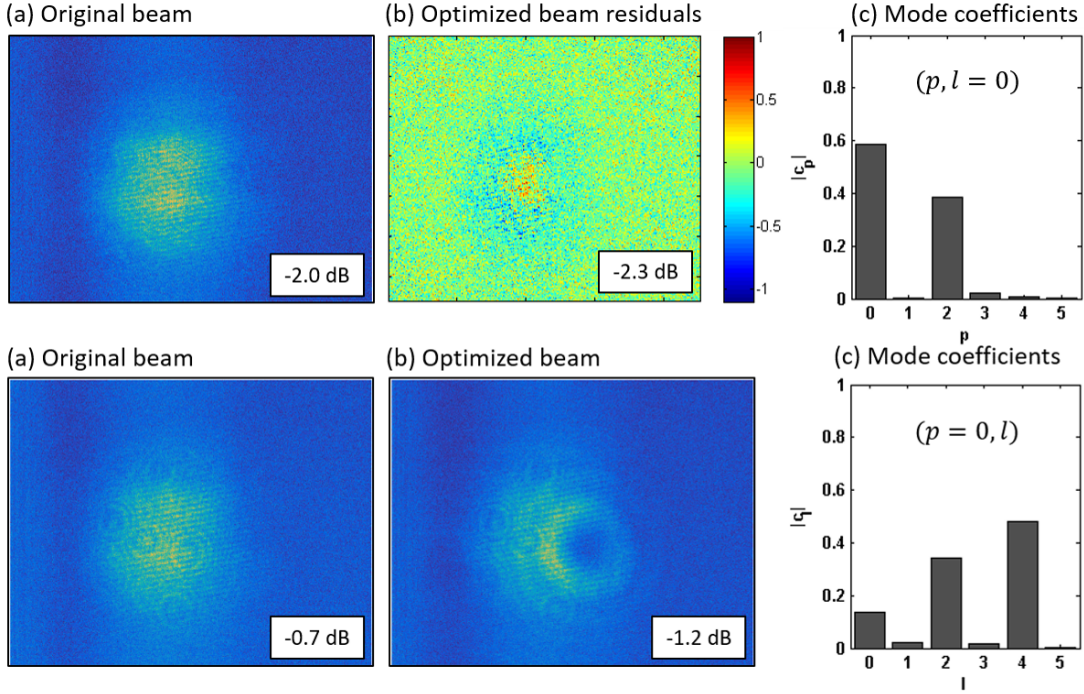


Figure 5-2: Top: Optimization run with optimal squeezing conditions. (a) Pump beam subject to a flat phase mask. (b) The residuals between the original beam and the optimized beam. (c) The LG mode coefficients used to create the optimized beam. Bottom: Optimization run with suboptimal squeezing conditions. (a) Pump beam subject to a flat phase mask. (b) The optimized beam. (c) The LG mode coefficients used to create the optimized beam.

(1) modes with $p = -5 : 5$ and $l = 0$, and (2) modes with $p = -10 : 10$ and $l = 0$. In our first studies, the temperature of the atomic cell was set to produce maximal squeezing, such that we had an atomic density of $9 \times 10^{12} \text{ cm}^{-3}$. Measured squeezing was 2.0 dB below shot noise. When the pump beam was reflected off of the SLM surface with a flat phase mask, the same squeezing remained. Running the optimization program with five modes (case 1), squeezing was improved to 2.3 dB below shot noise. The ten mode optimization (case 2) yielded -2.1 dB of squeezing.

Fig. 5-2, top left, is an image of the case 1 beam after interaction with the flat phase mask of the SLM and before interaction with the atoms. On the right is an image of the residuals between the flat phase mask beam and the optimized beam, where the phase mask has been set to display the combination of LG mode phase

shifts that optimize squeezing via the optimization algorithm. The change in the spatial structure of the beam is not visible to the eye, but we see some structure in the residuals. It seems the center of the beam grows weaker whereas the edges grow stronger. Indeed, this is what the mode coefficients used to create the optimized beam reveal: the LG_{00} and LG_{20} mode seem almost comparable in power.

We also studied the optimization process using a suboptimal atomic density for squeezing ($6 \times 10^{11} \text{ cm}^{-3}$). With a flat phase mask, the detection returned -0.7 dB of squeezing. When the optimization routine was run, the squeezing improved to -1.2 dB, a 0.5 dB improvement. Unlike before, it is visibly apparent that the optimized combination includes non-negligible higher order mode coefficients (Fig. 5-2, bottom right). The coefficients reveal that the new beam is in fact dominated by higher order modes. This large improvement in squeezing in an atomic density region that was once unusable for squeezing holds great promise. By optimizing the pump beam structure for different experimental conditions, PSR squeezing becomes highly more robust and versatile.

5.2 Local oscillator optimization

Previous work in our group demonstrated that excitement of higher order modes during the atom-light interaction may lead to imperfect mode match between the squeezed field and the local oscillator, limiting the amount of squeezing observed [7]. We moved the SLM after the squeezer to change the LO mode structure and see if we could find a good mode match between the LO and the squeezed vacuum. At optimal squeezing conditions, we measured -1.8 dB of squeezing with the SLM bypassed using mirrors. The beam was then reflected off of the surface of the SLM. When the SLM was powered off, squeezing is only slightly degraded. When the SLM was powered on with a flat mask, we measured -1.0 dB of squeezing, a great loss.

This loss may be explained by noise in the SLM. To alter the phase shift of the liquid crystals in the SLM, a voltage is applied. This voltage induces small oscillations in the liquid crystals. Such oscillation becomes a fluctuation in the phase distribution

of the mask, therefore changing the detected noise: by phase modulating the local oscillator, the detection scheme will cycle through quadratures and the average noise on average will be worse. Hence, unless we can resolve the oscillation effect, we will be unable to optimize the local oscillator spatial pattern. We continue to investigate this phenomenon.

Chapter 6

Quantum imaging

Previously, we have been unable to observe the squeezed vacuum beam directly with a camera as most cameras are limited by dark noise surpassing beam photon counts. In our work, we utilize a Princeton Instruments PIXIS series quantum noise-limited camera with sensors sitting in an ultra low temperature environment to reduce the thermal noise and the electronic noise. Each of the 1024×1024 pixels on the screen can detect photon counts of as low as a few hundred in a short exposure time. Each count corresponds to four photons incident on the pixel.

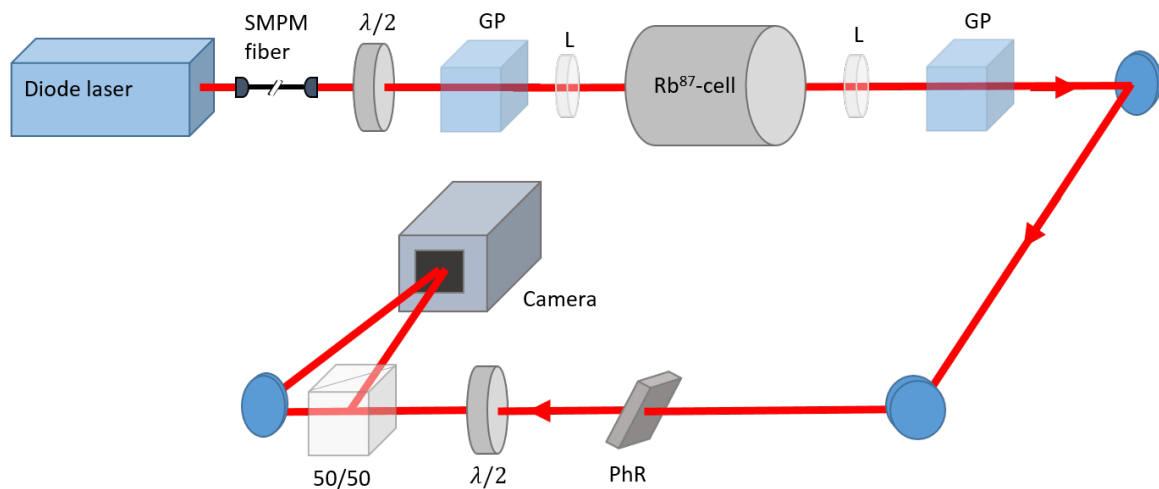


Figure 6-1: The experimental setup for measuring twin beams incident on the camera. A Glenn polarizer is placed after the atomic cell to allow for imaging of both the local oscillator and the squeezed vacuum. See Fig. 3-1 for defined abbreviations.

By analyzing beam images taken over a short period of time, we may identify the noise statistics of the beam. It is crucial that the images are taken on a short enough time scale such that classical noise in the laser amplitude does not dominate the noise distribution. Suppose we have a collection of images of a coherent beam. By taking photon statistics along the entire collection at each pixel, we find that the average photon number on each pixel is \overline{N} and variance is ΔN^2 . For the coherent beam, we would have

$$\frac{\Delta N^2}{\overline{N}} = 1$$

It is important to note that in practice, each count corresponds to four photons incident on the pixel, so we apply a multiplicative scaling.

6.1 Twin beam subtraction

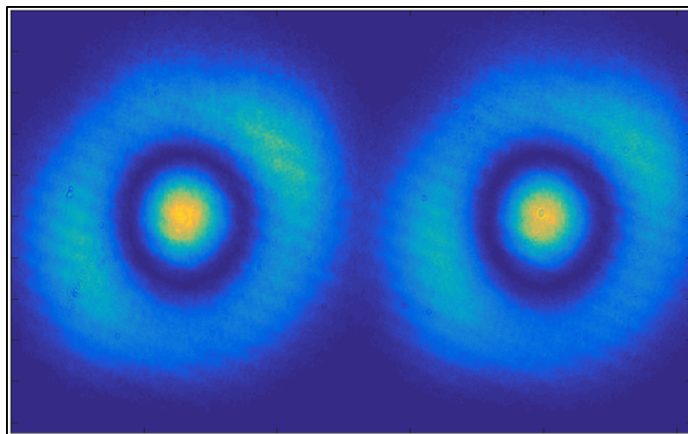


Figure 6-2: An image of the split beams incident on the camera. The polarizer has been set between the local oscillator and squeezed field polarizations to allow both beams through.

By observing the statistics of each pixel individually, we may identify noise “modes” in the beam. Our initial measurements revealed that classical noise was dominating our setup. Hence, we split the beam after the atoms into two beams and project both beams onto the camera screen (see Fig. 6-1). We developed a method for digitally overlapping and subtracting the two beams. In Fig. 6-2, we plot the beam intensities

corresponding to a beam where the polarization is between that of the local oscillator and the squeezed field. Again, we see the clear influence of higher order modes. Ideally, we want to determine whether the spatial modes of the beam carry different noise statistics.

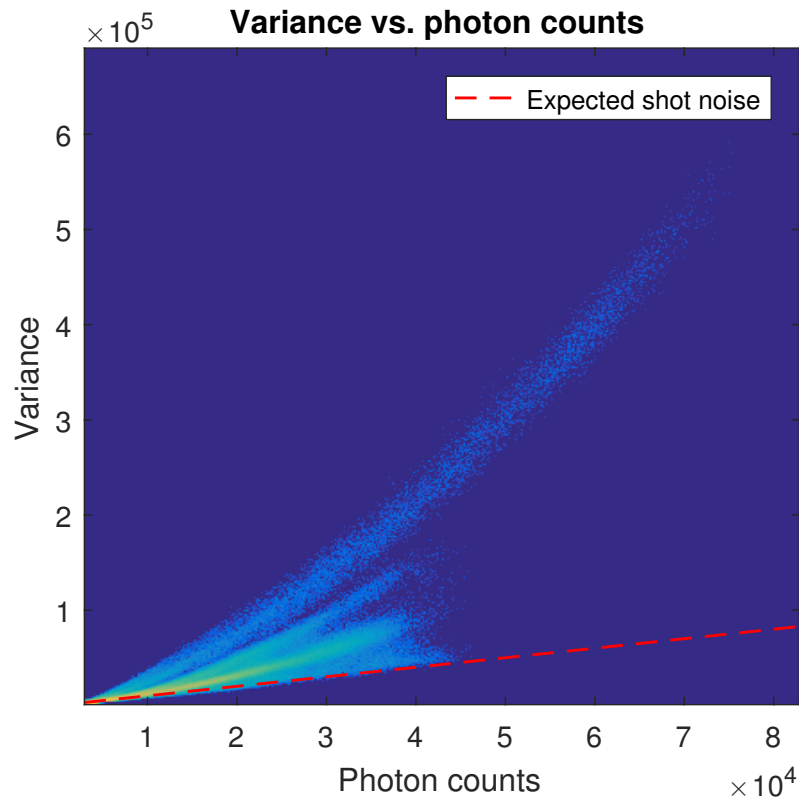


Figure 6-3: Variance versus photon counts for the twin beams incident on the camera. The variance statistics are taken from the subtracted beams. The intensity statistics are taken from the summed beams. The red line corresponds to the calibrated shot noise limit.

We plot the time-averaged noise statistics in Fig. 6-3. The calibrated shot noise limit that corresponds to a perfectly coherent beam is plotted. We see several distinct fumes in the variance versus intensity statistics. By matching the fumes to spatial patterns in the intensity profile, we identify a distinct “wedge” shape. This corresponds to the physical shutter of the camera flicking in and out of the beam. We find that it adds classical noise to our measurements. We cannot simply disable the shutter as the camera needs a dark period to process the images. To solve this

problem, we disabled the physical camera shutter and introduced an acoustic-optical modulator (AOM) before the SMPM fiber to diffract the beam away from the fiber port during camera processing time, *i.e.*, we implement a faster, more robust shutter.

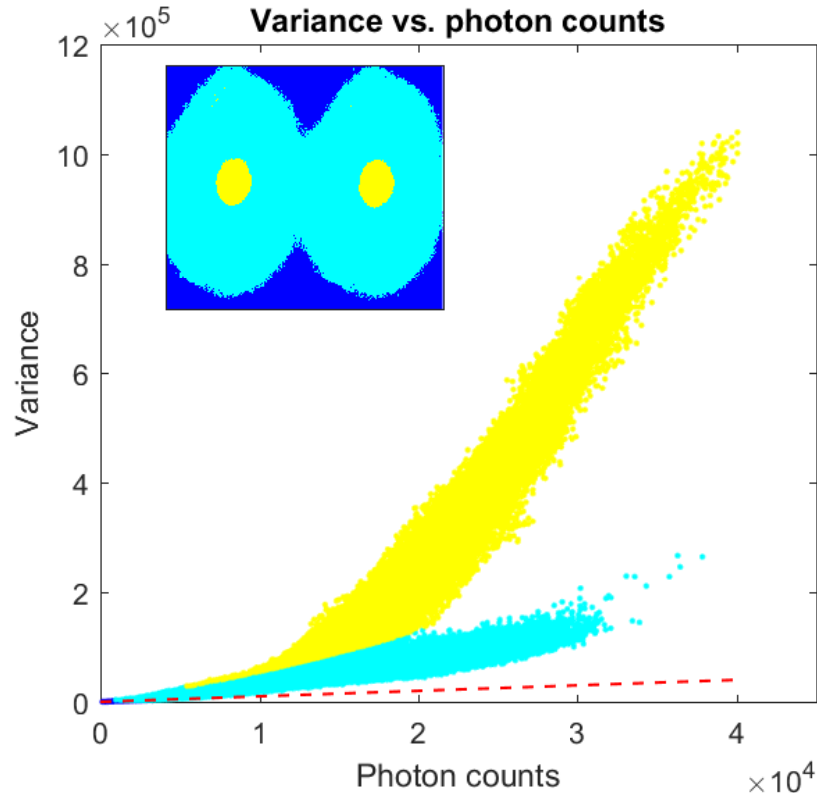


Figure 6-4: Variance versus photon counts for the twin beams after introducing an AOM in place of the physical camera shutter. The intensity map is plotted on top of the statistics to illustrate which pixels correspond with which noise fumes.

Using this new technique, we find that two of the four noise plues disappear, leaving us with a distinct linear plume and a distinct quadratic plume. In Fig. 6-4, we plot three different noise groups for the fumes: (1) dark noise (dark blue), (2) quadratic noise (yellow), and (3) linear noise (teal). We also plot the intensity image with pixels colored with the corresponding noise group. We find that there indeed exists a splitting in noise statistics in the beam mode structure. Referring back to Fig. 6-2, we compare the beam structure with the statistics. The center of the beam corresponds to the quadratic-with-intensity noise and the outer ring of the beam corresponds to linear noise. Typically, classical noise is quadratic whereas quantum noise is linear.

As of yet, we cannot say anything definitive about the noise modes: our analysis is preliminary and we are continuing to improve our detection methods.

6.2 Kinetic mode subtraction

In the time-averaging regime, we typically measure the beam across 1000 frames and this takes around ten minutes. Across ten minutes, our laser can drift substantially, introducing classical noise. Additionally, our twin beam subtraction scheme introduces additional spatial noise in our measurement. If the two beam splitter out ports have imperfections, the beams will diffract differently and exhibit differences in higher order noise. In addition, particles on the camera surface will cause differences in beam spatial structure. To avoid these complications, a superior imaging procedure would involve subtracting the beam from itself after a short enough time difference such that the beam cannot substantially shift.

To implement the measurement of images in quick succession, we implement a “kinetic mode” on the camera where the total active sensor area on the camera is divided into several frames. Here, the active area is rapidly shifted and processed. This allows us to take images separated by less than a few *ms*, sufficient to avoid excess noise from the laser. Hence each super frame contains five sub frames. We record 1000 image sequences and use the third and fourth sub frames for analysis, as they exhibit the most similar backgrounds. The beams were then subtracted, leaving us with 1000 super frames of subtracted beams.

Preliminary measurements using this new subtraction scheme exhibit extremely low noise. When analyzing a coherent beam with this method under specific conditions, we observe a noise versus intensity ratio consistent with theory

$$\frac{\Delta N^2}{N} = 1$$

Moving forward, we are working to measure the squeezed field using this new technique.

Chapter 7

Conclusions and outlook

In this report, we have demonstrated improved squeezing through mode optimization of the pump beam. The LG mode optimization improved squeezing by 0.3 dB. We have reason to be optimistic: it is likely that these studies may have only yielded a local minimum. Higher quality mode combinations that have not been probed by our optimization algorithm likely exist. We will next run a Hermite-Gaussian mode optimization, as this may be better suited for our square SLM screen.

We have also demonstrated that the power of the strong beam is redistributed from the Gaussian mode into higher order modes during the nonlinear light-atom interaction. By increasing the temperature and thus the density of the atoms, we may watch the power redistribute into other higher order modes. By using the spatial mode pattern identified in Fig. 4-2 as input for the SLM to tailor the pump beam, we may further improve squeezing.

In addition, we are now taking preliminary measurements of the beam spatial noise statistics using our quantum noise-limited camera. By monitoring the noise-intensity ratio across the pixels of the beam, we may discern which spatial portions of the beam squeeze more strongly than others. In this way, we may identify the squeezing mode pattern and study how its properties relate to overall squeezing. Ultimately, these studies are bringing us closer to understanding PSR squeezing and perhaps unlocking amounts of squeezing that have not previously been achieved with this method.

Our improved techniques for squeezing light are highly relevant to the cutting-edge

of many fields of research. Earth-based gravitational wave detectors rely on minute changes in optical resonator frequencies, resolving a fundamental quantum limit upon which gravitational waves might be detected. Reducing quantum noise moves us closer to a new era of observational astronomy [12]. In addition, quantum squeezing is applicable to innovative efforts in quantum computing. The squeezed state is ideal for probing quantum memories in order to retrieve their stored information [13]. Similarly, optical atomic clocks and magnetometers may be made more precise than ever before through utilization of squeezed input [9]. Squeezed light holds the key to the development of a modern tool set for the next stage of scientific progress.

Bibliography

- [1] C. M. Caves. Quantum-mechanical noise in an interferometer. *Phys. Rev. D*, 23(8):1693, April 1981.
- [2] H. Grote, K. Danzmann, K. L. Dooley an R. Schnabel, J. Slutsky, and H. Vahlbruch. First long-term application of squeezed states of light in a gravitational-wave observatory. *Phys. Rev. Lett.*, 110:181101, 2013.
- [3] P. Grangier, R. E. Slusher, B. Yurke, and A. LaPorta. Squeezed-light enhanced polarizaiton interferometer. *Phys. Rev. Lett.*, 50:2153–2156, November 1987.
- [4] M. Xiao, L. Wu, and H. J. Kimble. Detection of amplitude modulation with squeezed light for sensivity beyond the shot-noise limit. *Opt. Lett.*, 13(6):476–478, June 1988.
- [5] E. S. Polzik, J. Carri, and H. J. Kimble. Spectroscopy with squeezed light. *Phys. Rev. Lett.*, 68(20):3020–3023, May 1992.
- [6] A. B. Matsko, I. Novikova, G. R. Welch, D. Budker, D. F. Kimball, and S. M. Rochester. Vacuum squeezing in atomic media via self-rotation. *Phys. Rev. A*, 66:043815, October 2002.
- [7] M. Zhang, R. N. Lanning, Z. Xiao, J. P. Dowling, I. Novikova, and E. E. Mikhailov. Spatial multi-mode structure of atom-generated squeezed light. *Phys. Rev. A*, 93:013853, January 2016.
- [8] M. O. Scully and M. S. Zubairy. *Quantum Optics*. Cambridge University Press, Cambridge, 1997.
- [9] H. A. Bachor and T. C. Ralph. *A Guide to Experiments in Quantum Optics*. Wiley, NJ, 2004.
- [10] S. Barreiro, P. Valente, H. Failache, and A. Lezama. Polarization squeezing of light by single passage through an atomic vapor. *Phys. Rev. Lett.*, 84:033851, 2011.
- [11] M. Zhang, J. Souldanis, I. Novikova, and E. E. Mikhailov. Generating squeezed vacuum field with non-zero angular momentum. *Opt. Lett.*, 38:4833–4836, 2013.

- [12] K. Goda, O. Miyakawa, E. E. Mikhailov, S. Saraf, R. Adhikari, K. McKenzie, R. Ward, S. Vass, A. J. Weinstein, and N. Mavalvala. A quantum-enhanced prototype gravitational-wave detector. *Nature Physics*, 4:472–476, 2008.
- [13] E. E. Mikhailov and I. Novikova. Low-frequency vacuum squeezing via polarization self-rotation in rb vapor. *Opt. Lett.*, 33:12313–1215, 2008.